Characterization and modelling of switchable stop-band filters based on RF-MEMS and complementary split ring resonators

I. Gil[a], M. Morata[b], R. Fernández[a], X. Rottenberg[b] and W. De Raedtc[c]

[a] Department of Electronics Engineering, Universitat Politècnica de Catalunya, Terrassa E-08222, Spain

[b] Escuela Universitaria Salesiana de Sarriá, Barcelona E-08017, Spain

[c] IMEC, Leuven B-3001, Belgium

Abstract

In this work, we present the characterization and electrical modelling of a reconfigurable stop-band filter based on RF microelectromechanical systems (RF-MEMS) combined with metamaterial structures. The device consists of a coplanar waveguide (CPW) structure that combines complementary split ring resonators (CSRRs) and RF-MEMS varactor bridges operating at Q-band. A full electrical model for the description of the proposed structure is presented. The circuit model takes into account the electrical characteristics of the RF-MEMS, CSRRs and transmission line as well as the involved electromagnetic coupling and is used for accurate prediction of switchable filter response.

Keywords: Coplanar waveguide (CPW); RF-MEMS; Complementary split rings resonators (CSRRs); Metamaterials; Reconfigurable filters

1. Introduction

RF microelectromechanical systems (RF-MEMS) technology has been developed in different telecommunication applications with a certain degree of tunability. Devices such as switches, varicaps, tuners, tunable filters and antennas [1] and [2] are typically implemented by means of several lithographic steps which perform RF-MEMS in conventional distributed transmission lines.

Recently, some high-performance RF-MEMS switching devices have been combined with distributed MEMS transmission lines, in order to achieve current tuning capacitors requirements[3]. Alternatively, metamaterial transmission lines (i.e., artificial lines consisting of a host line loaded with reactive elements) have been revealed as good candidates in order to improve the performance of conventional distributed passive devices[4][5]. In order to predict the behaviour of these structures, several works have been developed to achieve accurate electrical models of RF-MEMS tunable filters[6][7] and tunable metamaterial transmission lines in PCB[8]. In this paper a switchable stop-band filter based on RF-MEMS metamaterials and its complete electrical model is shown. The filter operates at Q-band with potential applications in automotive radar and radio astronomy studies. The device combine the RF-MEMS tuning capacitor capabilities (working as capacitive switches) with the properties of the complementary split rings resonators (CSRRs)[9]. Such particles are metamaterial subwavelength resonators which allow constituting negative permittivity media and present a stop-band frequency response, near to the resonance frequency of the CSRRs. In order to validate the feasibility of the proposed filter and the proposal electrical model, a 4-stage periodic coplanar waveguide structure (CPW) loaded in its central strip with CSRRs embedding RF-MEMS varactor bridges has been fabricated and tested.

The paper is organized as follows: Section 2 introduces the switchable stop-band filter based on RF-MEMS metamaterials. The proposed electrical model of the filter is presented in Section 3, while the comparison between the experimental results and simulations is discussed in Section 4. Finally the conclusion is given in Section 5.

2. RF-MEMS metamaterials filter fabrication

Fig. 1(a) shows the layout of the proposed implementation. It consists of a 50 Ω CPW structure loaded with rectangular shaped CSRRs etched in the central strip and RF-MEMS bridges over them. The actual RF-MEMS structures implemented in the CSRRs uses an electrostatic floating bridge anchored on

the substrate in holes of the CPW ground planes. Under DC bias, bridge is in down state and contacts only the centre of the CPW strip. Therefore, the effective capacitance of the CSRRs can be modified, and hence, their intrinsic resonance frequency. As a result, a reconfigurable stop-band filter response is achieved. A stripped-down RF-MEMS technology using only three photolithographic steps[10] has been used to define a 4-stage periodic structure loaded with CSRRs and RF-MEMS. A 1μm thick Al layer is sputter-deposited and patterned on a 650 μm thick AF45 glass substrate ($\varepsilon r = 5.9$) to define mainly the CPW structures. The CSRRs have been performed by etching the central strip of the CPW. Then, a 3 μm thick sacrificial photoresist layer is spun and patterned to define the anchoring regions of the MEMS devices before a second Al layer is deposited and patterned in the same way as the first one. Therefore, the MEMS beams are defined. Finally, the sacrificial photoresist is ashed to release the devices. Fig. 1(b) shows the photograph of the actual implemented reconfigurable filter.

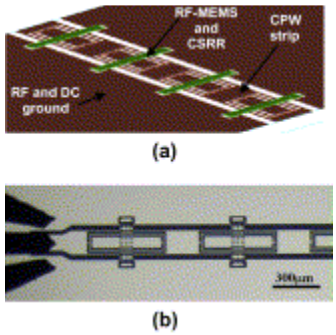

Fig. 1. (a) Layout of the fabricated switchable notch filter. (b) Microphotograph of the first two stages of the device under test with RF probes. The down state corresponds to the application of an actuation voltage to the strip line of the CPW; in the up-state, no actuation voltage is applied.

3. Proposed electrical model

The detailed dimensions of the CSRR/RF-MEMS unit cell and the proposed lumped-element equivalent circuit model are shown in Fig. 2(a) and (b), respectively. The RF-MEMS bridges are modelled by means of a lumped RLC series circuit, where C_M corresponds to a variable capacitance (having an up-state and a down state value), L_M is the bridge inductance and the resistor R_M involves the microelectromechanical system losses. The anchoring capacitance of the CPW holes is modelled by C_H. The CPW line is described by means of the per-section inductance, L, and capacitance, C (their actual value must be slightly corrected due to the coupling with the CSRR). The etched CSRRs are modelled by means of a parallel RLC tank[4], L_C and C_C being the reactive elements which constitute the intrinsic resonance frequency of the resonators and R_C takes into account the eventual losses associated with the resonator. CSRRs are directly connected to the host line and electrically coupled to the capacitance of the RF-MEMS. Therefore, the intrinsic resonance frequency of the subwavelength resonators is directly affected by the RF-MEMS actuation. In fact, when C_M is tuned the electrical properties of CSRRs are modified so that their resonance frequency. In order to take into account this fact, the capacitor C_C has been represented dependant on the capacitor C_M. Since the actual RF-MEMS device is anchored directly on the substrate in holes of the CPW ground planes, the anchoring capacitance can be neglected due to its low impact. In order to extract the different parameters of the electrical model, the problem is analyzed sequentially due to the number of involved variables. First, the CPW reactive elements, L and C, can be extracted by means of a conventional transmission line calculator (Agilent Line Calc) in the absence of the CSRR and the bridge. Second, an electromagnetic simulation of the AF45 glass substrate (using the commercial Agilent Momentum) is performed by taking into account the layout of the CSRR etched in the CPW (with no RF-MEMS). The evaluation of the resonance frequency of the CSRR (tank $L_C C_C$) has been used in order to determine the value of its reactive elements, according (1),

$$f_o = \frac{1}{2\pi\sqrt{L_C C_C}}.$$

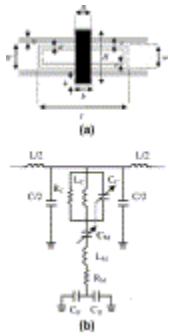

Fig. 2. (a) Unit cell of the CSRR/RF-MEMS loaded CPW, with slot regions of the CPW depicted in grey and RF-MEMS in black. Actual dimensions are: $c = d = 10$ μm, $l = 480$ μm, $w = 130$ μm, $W = 150$ μm, $G = 30$ μm, $B = 80$ μm, $b = 100$ μm, $h = 40$ μm and $H = 290$ μm. The distance between adjacent CSRRs is 220 μm. (b) Lumped-element equivalent circuit for the unit cell, including losses.

On the other hand, C_M can be estimated in a first approximation by the well-known parallel plate capacitance equation. The effective cross area of the RF-MEMS over the CPW and the CSRR has been considered. Finally, C_M and L_M have been determined from electromagnetic simulation of the CPW/RF-MEMS (with no CSRRs) layout. In order to achieve all the reactive elements, the system is assumed lossless for simplicity and, therefore, $R_M = R_C = 0$ in a first stage. However, even this procedure leads to a good agreement with respect to the resonance frequency and tuning range of the device, losses must be considered in order to fit the actual quality factor, as will be shown in next section. Therefore, in a second stage, R_M is derived according [1], whereas RC is considered as a fitting parameter (the starting value of RC is extracted from the electromagnetic simulation of the CSRR without RF-MEMS and it requires a slight tuning when the overall structure is considered). Table 1 summarizes the extracted model parameters according this procedure. Note that two values for C_C and C_M have been considered: C_{MU} and C_{MD} describe the up and down MEMS state, respectively; C_{CU} and C_{CD} corresponds to the value of the CSRR capacitor for the up and down state. C_{CU} has been obtained by means of the electromagnetic simulation and corresponds to the intrinsic capacitance value of the CSRR. This fact points out that in the up-state there is no significant coupling between RF-MEMS and CSRR. However, in the down state, the actual

distributed capacitance of the RF-MEMS modifies the electrical characteristics of the CSRRs and significant electric coupling between the bridges and the CSRRs is observed. This phenomenon is modelled by increasing the value of the CSRR capacitance in down state ($C_{CD} > C_{CU}$).

Table 1.

Equivalent circuit model parameters.

L (nH)	C (fF)	L_C (pH)	C_{CU} (pF)	C_{CD} (pF)	R_C (Ω)	L_M (pF)	C_{MU} (fF)	C_{MD} (fF)	R_M (Ω)	C_H (pF)
0.149	59	30	0.27	0.41	90	38	65	111	0.5	0.4

4. Simulated and experimental results

In order to validate the proposed filter and its lumped model we have compared the electric simulations of the 4-stages CSRR/RF-MEMS filter with the corresponding layout electromagnetic simulations and measurements. The measurement setup consists of a HP8510C vector network analyzer and G–S–G test probes having coaxial connectors (type 2.4 mm). [Fig. 3] and [Fig. 4] show the comparison between the measured data (up to 50 GHz), electromagnetic simulations and the proposed lumped model insertion (S21) and return (S11) losses. Both, the up and down state have been electromagnetically simulated by considering a parallel plate to the host line (MOMENTUM corresponds to a 2.5D simulator). Layout simulation has been carried out by considering planar plate heights of 0.5 μm (down state) and 2 μm (up-state), respectively and no losses have been assumed ($R_M = R_C = 0$). As expected, the structure exhibits stop-band behaviour with reconfigurable capability. The simulated frequency range corresponds to 39–48.8 GHz (Q-band), which implies to a switching range of roughly 20%. As can be seen, good matching level between the involved notch frequencies concerning the model prediction is achieved. However, the band edges, related with the quality factor, as well as the rejection level are not correctly reproduced due to the intrinsic lossless simplicity. Electromagnetic simulated rejection levels are IL < −50 dB

whereas model predicts higher notch rejection levels. Regarding experimental results, the RF-MEMS have been subjected to actuation voltage, caused by an external polarization, from 17 V (down state) to 0 V (up-state). Fig. 5(a) and (b) illustrates the comparison between full equivalent circuit model including losses and experimental insertion (S21) and return (S11) losses. A significant agreement is achieved, not only concerning the tuning range (experimental values are 39–48.1 GHz, whereas model correspond to 38.9–47.5 GHz), but also in terms of rejection level (experimental IL_D = −43 dB; IL_U = −40.9 dB and model IL_D = −50.4 dB; IL_U = −40.2 dB) and quality factor (experimental Q_D = 30.9; Q_U is not determined due to the limitation up to 50 GHz in the setup, and model Q_D = 29.7; Q_U = 29.5). These results reveal the need to include losses in the model as well as the dependence on the capacitors C_M and C_C.

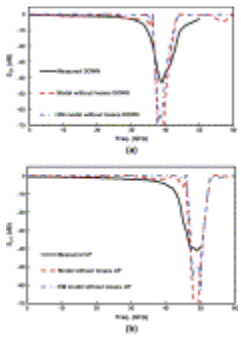

Fig. 3. Insertion losses corresponding to the down state (a) and the up-state (b) of the filter. Measurement data, electromagnetic simulations and electrical model are shown. Simulations are assumed to be lossless.

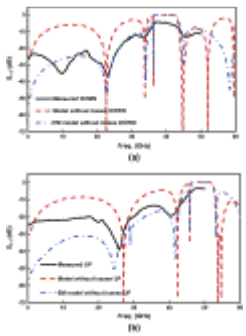

Fig. 4. Return losses corresponding to the down state (a) and the up-state (b) of

the filter. Measurement data, electromagnetic simulations and electrical model are shown. Simulations are assumed to be lossless.

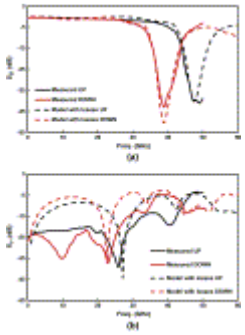

Fig. 5. Comparison between the full electrical model (including losses) and the experimental data for the designed stop-band reconfigurable CSRR/RF-MEMS filter. Insertion (a) and return losses (b) are depicted.

5. Conclusion

In summary, a reconfigurable stop-band filter based on CSRR/RF-MEMS cells is performed and described by means of a full lumped equivalent circuit. A high degree of accuracy of the model has been demonstrated by comparison with device measurements in terms of switching frequency range (20%), quality factor (>30) and rejection level (<−40 dB). This work opens the door to the design of millimetre wave components based on the combination of RF-MEMS and metamaterial-based technologies.

Acknowledgement

This work was supported by the Spain-MICINN under Project TEC2009-09994 and AGAUR 2009 SGR 1425.

References

[1] G.M. Rebeiz, RF MEMS: Theory, Design and Technology, John Wiley & Sons (2003).

[2] X. Rottenberg, P. Soussan, S. Stoukatch, P. Czarnecki, B. Nauwelaers, G. Carchon, I. De Wolf, W. De Raedt, H.A.C. Tilmans, RF-MEMS technology platform for agile mobile and satellite communications, in Proceedings of the European Microwave Conference, Manchester, UK, 2006, pp. 1723–1726.

[3] M.F. Bolaños, J.P. Carrier, P. Dainesi and A.M. Ionescu, *Microelectronic Engineering* **85** (2008), pp. 1039–1042.

[4] J. Bonache, I. Gil, J. García-García and F. Martín, *IEEE Transactions on Microwave Theory and Techniques* **54** (2006), pp. 265–271.

[5] J. García-García, F. Martín, E. Amat, F. Falcone, J. Bonache, I. Gil, T. Lopetegi, Miguel A.G. Laso, A. Marcotegui, M. Sorolla and Ricardo Marqués, *IEEE Transactions on Microwave Theory and Techniques* **53** (2005), pp. 1997–2006.

[6] K. Entesari and G.M. Rebeiz, *IEEE Transactions on Microwave Theory and Techniques* **53** (2005), pp. 2566–2571.

[7] K. Entesari, K. Obeidat, A.R. Brown and G.M. Rebeiz, *IEEE Transactions on Microwave Theory and Techniques* **55** (2007), pp. 2399–2405.

[8] I. Gil, J. Bonache, J. García and F. Martín, *IEEE Transactions on Microwave Theory and Techniques* **54** (6) (2006), pp. 2665–2674.

[9] F. Falcone, T. Lopetegi, M.A.G. Laso, J.D. Baena, J. Bonache, R. Marqués, F. Martín and M. Sorolla, *Physical Review Letters* **93** (2004), p. 197401.

[10] X. Rottenberg, S. Brebels, P. Ekkels, P. Czarnecki, P. Nolmans, R.P. Mertens, B. Nauwelaers, R. Puers, I. De Wolf, W. De Raedt and H.A.C. Tilmans, *Journal of Micromechanics and Microengineering* **17** (2007), pp. S204–S210.